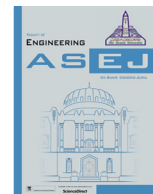




Contents lists available at ScienceDirect

Ain Shams Engineering Journal

journal homepage: www.sciencedirect.com

Exploration of 3D stagnation-point flow induced by nanofluid through a horizontal plane surface saturated in a porous medium with generalized slip effects

Yangyang Yu^a, Umair Khan^{b,c}, Aurang Zaib^{d,*}, Anuar Ishak^b, Iskandar Waini^e, Zehba Raizah^f, Ahmed M. Galal^{g,h}

^a School of Mathematics and Statistics, Xuzhou University of Technology, Xuzhou 221018, China

^b Department of Mathematical Sciences, Faculty of Science and Technology, Universiti Kebangsaan Malaysia, UKM Bangi 43600, Selangor, Malaysia

^c Department of Mathematics and Social Sciences, Sukkur IBA University, Sukkur 65200, Sindh, Pakistan

^d Department of Mathematical Sciences, Federal Urdu University of Arts, Science & Technology, Gulshan-e-Iqbal Karachi 75300, Pakistan

^e Fakulti Teknologi Kejuruteraan Mekanikal dan Pembuatan, Universiti Teknikal Malaysia Melaka, Hang Tuah Jaya, 76100 Durian Tunggal, Melaka, Malaysia

^f Department of Mathematics, College of Science, Abha, King Khalid University, Saudi Arabia

^g Mechanical Engineering Department, College of Engineering, Prince Sattam Bin Abdulaziz University, Wadi addawaser 11991, Saudi Arabia

^h Production Engineering and Mechanical Design Department, Faculty of Engineering, Mansoura University, P.O. 35516, Mansoura, Egypt

ARTICLE INFO

Article history:

Received 29 March 2022

Revised 20 May 2022

Accepted 13 June 2022

Available online 04 July 2022

Keywords:

Three-dimensional flow

Nanofluid

Generalized slip effects

ABSTRACT

Heat transfer enhancement is a contemporary challenge in a variety of fields such as electronics, heat exchangers, bio and chemical reactors, etc. Nanofluids, as innovative heat transfer fluids, have the potential to be an efficient tool for increasing energy transport. This benefit is obtained as a result of an enhancement in effective thermal conductivity and an alteration in the dynamics of fluid flow. Thus, this paper is concerned with heat transfer enhancement via nanofluids. The intention is to find numerical double solutions to the 3D stagnation-point flow (SPF) and heat transfer incorporated nanoparticles in a porous medium with generalized slip impacts. Appropriate similarity variables are used to non-dimensionalize the leading equations, which are then numerically solved using the three-stage Lobatto IIIa integration formula. The impacts of different parameters on the dynamics of flow and characteristics of heat transfer induced by nanofluids in the presence of an unsteady parameter, nanoparticle volume fraction, velocity slip parameter, and porosity parameter are investigated. Based on the latest findings, it is closed that the velocity slip improves the heat transfer as well as shear stress in the axial direction in both solutions, while the shear stress behaves oppositely in the respective lateral direction. In addition, the velocity profile remarkably enriches for both branch solutions, while the temperature distribution elevates for the upper branch and declines for the lower branch owing to the larger porosity parameter.

© 2022 THE AUTHORS. Published by Elsevier BV on behalf of Faculty of Engineering, Ain Shams University. This is an open access article under the CC BY-NC-ND license (<http://creativecommons.org/licenses/by-nc-nd/4.0/>).

1. Introduction

The introduction of nanofluids has turned out to be a promising substitute for conventional heat handling fluids in heat transfer

technology, such as engine oil, ethylene glycol, water, and so on. Nano-sized compact particles are dispersed uniformly and stably in regular fluids to produce 'nanofluids,' which have improved transport and thermal properties over the base fluids. Nanofluids have unique features which sound a fantastic advancement in several industrial and engineering applications, which include micro-electronics, domestic refrigerators, hybrid-powered engines, chillers, and even significant specialized military gadgets. Choi and Eastman [1] initiated the first work on nanofluids and their potential to suspend nano-sized particles in conventional fluids due to their increased thermal conductivity as well as a factor of heat transfer rate. Khanafer et al. [2] investigated the dominated buoyancy flow via a 2D enclosure with the suspension of the

* Corresponding author.

E-mail address: zaib20042002@yahoo.com (A. Zaib).

Peer review under responsibility of Ain Shams University.



<https://doi.org/10.1016/j.asej.2022.101873>

2090-4479/© 2022 THE AUTHORS. Published by Elsevier BV on behalf of Faculty of Engineering, Ain Shams University.

This is an open access article under the CC BY-NC-ND license (<http://creativecommons.org/licenses/by-nc-nd/4.0/>).

Nomenclature

x_a, y_a, z_a	Cartesian coordinates (m)
u_a, v_a, w_a	Velocity components (m/s)
v_{ey_a}, u_{ex_a}	Ambient velocity in the axial and lateral directions (m/s)
t_a	Time (s)
T_a	Temperature (K)
k	Thermal conductivity (kg m/s ³ K)
A_a, B_a	Arbitrary constants
T_∞	Ambient temperature (K)
α_A	Unsteadiness parameter
T_w	Temperature at the wall surface (K)
Pr	Prandtl number
$F(\xi)$	Dimensionless velocity in the lateral direction
$G(\xi)$	Dimensionless velocity in the axial direction
C_a	Saddle/Nodal indicative parameter
K^*	Positive arbitrary constant
m_a	Porous media permeability parameter
$S(\xi)$	Dimensionless temperature
C_{fx_a}, C_{fy_a}	Coefficient of skin friction in the axial and lateral directions
Nu_{x_a}	Local Nusselt number
Re_{x_a}, Re_{y_a}	Local Reynolds numbers
<i>Greek symbols</i>	
μ	Dynamic viscosity (Kg/m s)
ρ	Density (Kg/m ³)
K_a	Porous medium permeability (m ²)
(ρc_p)	Specific heat capacity at constant pressure (m ² /s ² K)
σ_u	Tangential momentum accommodation coefficient
λ_a	Time-dependent coefficient of the free path
φ	Nanoparticle volume fraction
λ^*	Arbitrary constant
δ_a	Dimensionless velocity slip factor

ν	Kinematic viscosity (m ² /s)
ξ	Pseudo-similarity variable

Acronyms

3D	Three-Dimensional
SP	Stagnation point
CuO	Copper oxide
PDEs	Partial differential equations
LBS	Lower branch solution
ODEs	Ordinary differential equations
SL	Slip length
SST	Shear stress
BC	Boundary condition
SR	Shear rate
MHD	Magneto-hydrodynamic
UBS	Upper branch solution
CP	Critical point

Subscripts

nf	Nanofluid
s	Solid nanoparticles
f	Base fluid
CuO	Copper oxide nanoparticles
∞	Ambient condition
w	Condition at surface
∞	Ambient condition

Superscript

'	Differentiation with respect to ξ .
---	---

nanoparticle. The mechanism of free convection in a rectangular domain through a convectively heated enclosure equipped with nanoparticles was inspected numerically by Oztop and Abu-Nada [3]. Motsumi and Makinde [4] investigated viscous flow induced by nanofluids over a movable penetrable plate with viscous dissipation and radiation consequences. The impact of a magnetic field on the fluid flow near a stagnation-point containing nanofluid past a stretchable sheet with irregular radiation was examined by Farooq et al. [5]. He observed that the Nusselt number enhances due to the conjunction of nanoparticle volume fraction. Naramgari and Sulochana [6] published a work of heat transfer and magneto flow through a permeable stretchable/shrinkable sheet induced by a nanofluid. According to their findings, the magnetic parameter shrinks the boundary-layer flow, heat transfer rate, and friction factor on the stretchable surface. The influences of viscous dissipation and Joule heating on the radiative flow comprising nanofluid past a stretchable sheet with the magnetic field were inspected by Daniel et al. [7]. The coefficient of heat transfer and thermal conductivity of nano liquid within the convectational fluid significantly improved were observed by Kumar et al. [8]. The effectiveness of synthesized nanosilica particles in diminishing fines migration during hydraulic fracturing was explored via Moghadasi et al. [9]. Abbas et al. [10] elaborated on the features of the swirling flow of a non-Newtonian Oldroyd-B fluid through a convectively heated surface with heat generation/ absorption incorporated nanofluid. They observed that mechanisms of mass and heat transport for von Kármán swirling flow have a substantial effect on the rate of mass and heat transfer. Turkyilmazoglu [11] presented the interaction phenomena of scattered particles within the fluid past

a stretching rotated disc. He observed that cooling of the disk's surface can be reached by enhancing the rotation number. The physical properties of laminar 2D MHD flow of Sisko fluid induced by nanofluid past a radial stretchable/shrinkable surface by a zero mass-flux were scrutinized by Khan et al. [12]. They reported double answers for a particular range of moving parameter. Ramesh et al. [13] explored the thermal features by incorporating thermal radiation, activation energy, and magnetic influence through nanofluid to enhance the performance of mass and heat transfer. Turkyilmazoglu [14] discussed the features of mass and heat transfer by considering distinct geometries by employing Buongiorno nanofluid model. Khan et al. [15] discussed the impact of activation energy and viscous dissipation on the Marangoni convection flow in a Darcy-Forchheimer medium induced by a hybrid nanofluid. They found that the temperature uplifts due to the Eckert number. The features of thermo-hydraulic on pulsating flow in the presence of heat transfer as well as in absence of heat transfer induced by nanofluid were investigated by Esfe et al. [16]. Turkyilmazoglu [17] presented the features of enhancement of heat transfer by employing non-Fourier heat flux to adjust the finite time travel of heat. Bahiraei and Mazaheri [18] numerically investigated the irreversibility and hydrothermal properties of an eco-friendly GO-based nanofluid inside an innovative spiral heat sink. They observed that the spiral heat sink can enhance thermal performance with less pressure loss intensifying and less irreversibility than the sinuous heat sink. Song et al. [19] reported the exploration of the bioconvection radiative flow of micropolar fluid through a rotating off-centered disk in a Darcy law induced by a nanofluid. Khan et al. [20] examined the bio-convection effect in the cross-

flow and stream-wise directions containing nanofluid. The properties of heat generation, and thermal radiation through a heated duct with the Rabinowitsch fluid were discussed by Chu et al. [21]. Bahiraei et al. [22] studied the potential of a triple pipe heat exchanger operating including a water-based alumina nanofluid using a novel crimped spiral rib. They examined that the thought of employing crimped spiral rib is significant in nanofluids' thermal irreversibility. Recently, Mazaheri et al. [23] evaluated the features of the second law of a four-layer counter flow micro-channel heat exchanger by incorporating water-based Al_2O_3 nanofluid in a 3D two-phase analysis.

The no-slip condition is insufficient when the accompanying liquid is particulate, such as polymer solutions, suspensions, emulsions, and foams, or when the surface is adequately smooth. Navier [24] and Maxwell [25] initially suggested the linear boundary restriction defining the component of tangential momentum accommodation at the ground wall is proportional to the shear stress (SST). According to Matthews and Hills [26], the slip length is signified as proportionality constant. The impact of partial slip on the surface of the planar flow through stretching motion was examined by Wang [27] and presented an exact solution. On the other hand, Thompson and Troian [28] proposed that the slip length (SL) is a function of shear rate rather than a constant based on molecular dynamic simulation. They discovered that while the slip length behavior is similar to that of Navier's slip condition at low SR, it is no longer applicable at high SR because the SL grows rapidly with shear rate. The relationship between SL and SR is erratic and therefore, the suggested BC is non-linear and consequently, the suggested BC is nonlinear including for the viscous flows. Matthews and Hill [29] utilized this slip condition to investigate the few viscous flows. The impact of general slip conditions on stretchable flows was surveyed by Sajid et al. [30]. Khan et al. [31] considered the thermal as well as hydrodynamic slip conditions on the natural free convection flow induced by nanofluid past a vertical plate with double diffusion. The impact of erratic slip condition on the Couette flow with the behavior of Newtonian fluid through double rotated cylinders was inspected by Power et al. [32]. Recently, Khashi et al. [33] investigated the influences of CBCs and slip on a three-dimensional flow of a hybrid nanofluid through a stretchable/shrinkable sheet.

The exploration of flows near the stagnation-point has captured the attention of many engineers and analysts because of its significant applications in mechanical and engineering processes. Hiemenz [34] was the first to investigate the 2D stagnation-point flow past a static semi-infinite wall, employing a similarity technique to shrink the Navier-Stokes equations to non-linear ODEs. Homann [35] extended this problem to the case of axisymmetric stagnation point flow. Mahapatra and Gupta [36,37] investigated Hiemenz as well as Homann's problems past a stretchable sheet. The axisymmetric, as well as 2D stagnation point flow in a viscous fluid towards a shrinking sheet was investigated by Wang [38]. He found double solutions. Since then several researchers [39–43] examined the stagnation point flows with different aspects.

A porous media can be defined as a material with passages that are filled with fluid flowing in gaseous or liquid forms. Intercrystalline and intergranular porosity are distinguished by differences in the cavern and molecular interstices. As a result, the potency of porous media has received considerable attention in processing applications, and in academic research. The characteristics of the medium, such as permeability, thermal conductivity, and heat capacitance are mostly determined by the solid matrix, pores structure, and media porosity. Transfer and porous media are gratifying increasing appealing in the analysis and designing of heat transfer and heat exchanger devices. When the fluid travels via porous media, it comes into contact with its large surface area, and the rate of heat transfer in a fluid is increased due to the tortu-

ous structure of the media. Furthermore, porous media is utilized to cool or heat fluids and to strengthen fluid thermal conductivity. Ahmad and Pop [44] studied the impact of suction on the buoyancy effects from a flat vertical plate induced by nanofluids embedded in porous media and reported double solutions. The impact of the magnetic field on the fluid flow comprising nanofluid embedded in a source of the porous media was inspected by Sheikholeslami et al. [45]. They utilized Darcy models as well as the KKL approach to investigate nanofluid in porous media through the cavity. Bakar et al. [46] investigated mixed convective radiative flow past a cylinder containing nanofluid induced in a porous media source. Turkyilmazoglu [47] investigated the entropy and velocity slip features through thermal transport via a Brinkman-Darcy model and presented a closed-form solution. The explorations of nanofluid saturated in a porous medium are further disclosed in refs. [48–54].

The novelty of the problem is to obtain the numerical dual solutions of radiative flow near a 3D SP comprising water-based copper-oxide nanoparticles in a Darcy porous media with generalized slip effects in this paper as the authors are motivated by the cited literature. We mainly spotlight in this work on the upshot of generalized slip associated with time-dependent free path and tangential momentum accommodation on the leading system as well as thermal convection. To the best knowledge of the authors, such a study has not previously been reported in the literature.

2. Mathematical modeling of the problem

Consider an unsteady, incompressible viscous 3D flow towards an SP comprising nanofluid past a horizontal surface saturated in a porous media. The nanofluid is made up of CuO nanoparticle that is uniformly dispersed in the convectational fluid water. It is assumed that a system of Cartesian coordinate (x_a, y_a, z_a) through the origin O is located in the region of onward stagnation with x_a and y_a coordinates along the plane surface of the body. The fluid flow is inhabited by $z_a > 0$ perpendicular to the surface of the object at O (see Fig. 1). The region of flow towards the SP is classified into two categories: region of potential flow and varying region of velocities provoking the boundary-layer. Unsteadiness in the fluid flow is imparted when the ambient velocity displays impulsive motion or varies arbitrarily with time. Instigating the above assumptions, the time-dependent requisite governing equations in terms of PDEs can be determined using the boundary-layer approximations as [55].

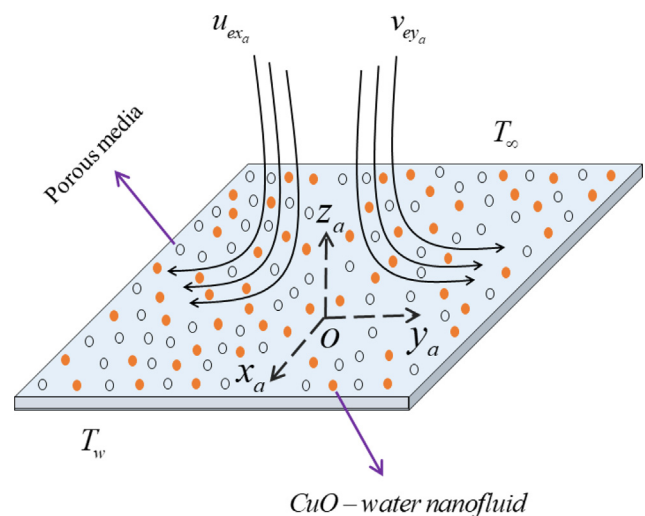


Fig. 1. Geometry of the physical model.

$$\frac{\partial u_a}{\partial x_a} + \frac{\partial v_a}{\partial y_a} + \frac{\partial w_a}{\partial z_a} = 0, \tag{1}$$

$$\begin{aligned} \frac{\partial u_a}{\partial t_a} + u_a \frac{\partial u_a}{\partial x_a} + v_a \frac{\partial u_a}{\partial y_a} + w_a \frac{\partial u_a}{\partial z_a} &= \frac{\partial u_{exa}}{\partial t_a} + u_{exa} \frac{\partial u_{exa}}{\partial x_a} + \frac{\mu_{nf}}{\rho_{nf}} \frac{\partial^2 u_a}{\partial z_a^2} \\ &\quad - \frac{\varepsilon_a \mu_{nf}}{K_a \rho_{nf}} (u_a - u_{exa}), \end{aligned} \tag{2}$$

$$\begin{aligned} \frac{\partial v_a}{\partial t_a} + u_a \frac{\partial v_a}{\partial x_a} + v_a \frac{\partial v_a}{\partial y_a} + w_a \frac{\partial v_a}{\partial z_a} \\ = \frac{\partial v_{eya}}{\partial t_a} + v_{eya} \frac{\partial v_{eya}}{\partial y_a} + \frac{\mu_{nf}}{\rho_{nf}} \frac{\partial^2 v_a}{\partial z_a^2} - \frac{\varepsilon_a \mu_{nf}}{K_a \rho_{nf}} (v_a - v_{eya}), \end{aligned} \tag{3}$$

$$\frac{\partial T_a}{\partial t_a} + u_a \frac{\partial T_a}{\partial x_a} + v_a \frac{\partial T_a}{\partial y_a} + w_a \frac{\partial T_a}{\partial z_a} = \frac{k_{nf}}{(\rho c_p)_{nf}} \frac{\partial^2 T_a}{\partial z_a^2}, \tag{4}$$

subject to the boundary conditions (BCs) are.

$$\left. \begin{aligned} u_a &= u_{slip}, v_a = v_{slip}, w_a = 0, T_a = T_w \text{ at } z_a = 0, \\ u_a &\rightarrow u_{exa}, v_a \rightarrow v_{eya}, w_a \rightarrow W_a, T_a \rightarrow T_\infty \text{ as } z_a \rightarrow \infty. \end{aligned} \right\} \tag{5}$$

where (u_a, v_a, w_a) refers to components of velocity in the x_a, y_a, z_a directions, T_a signifies temperature, σ_u denotes the tangential momentum accommodation coefficient, and λ_a presents the time-dependent coefficient of the free path. It is worth mentioning that u_{slip} and v_{slip} are signified as the slip velocities at the plate and are demonstrated as.

$$u_{slip} = \frac{2 - \sigma_u}{\sigma_u} \lambda_a \frac{\partial u_a}{\partial z_a}, v_{slip} = \frac{2 - \sigma_u}{\sigma_u} \lambda_a \frac{\partial v_a}{\partial z_a}. \tag{5a}$$

The components of external flow velocity over 3D surfaces of the body are denoted by:

$$u_{exa} = \frac{A_a x_a}{1 - \alpha_A t^*}, v_{eya} = \frac{B_a y_a}{1 - \alpha_A t^*}, t^* = A_a t_a. \tag{6}$$

where α_A represents the unsteadiness with $\alpha_A < 0$ and $\alpha_A > 0$ are signified as decelerating flow and accelerating flow, respectively. Also, it is presumed that the surface temperature T_w and free stream temperature T_∞ are constants near the stagnation point.

The effective viscosity, density, thermal conductivity, and heat capacitance of nanofluid are demonstrated as.

$$\begin{aligned} \frac{\mu_{nf}}{\mu_f} &= (1 - \varphi)^{-2.5}, \frac{\rho_{nf}}{\rho_f} = \varphi \left(\frac{\rho_s}{\rho_f} \right) + (1 - \varphi), \frac{k_{nf}}{k_f} = \frac{(k_s + 2k_f) - 2\varphi(k_f - k_s)}{(k_s + 2k_f) + \varphi(k_f - k_s)}, \\ \frac{(\rho c_p)_{nf}}{(\rho c_p)_f} &= \varphi \left(\frac{(\rho c_p)_s}{(\rho c_p)_f} \right) + (1 - \varphi). \end{aligned} \tag{7}$$

where φ namely corresponds to the solid nanoparticles volume fraction and is equal to the sum of the copper oxide nanoparticle (CuO) and the regular (viscous) fluid (H₂O). Additionally, k_f, ρ_f, μ_f and $(\rho c_p)_f$ indicate the thermal conductivity, density, dynamic viscosity, and the specific heat capacity at a constant pressure of the regular (viscous) fluid, respectively, while k_s, ρ_s and $(\rho c_p)_s$ are the respective quantities of the solid nanoparticles. Moreover, the subscript s and f is classified as the solid nanoparticles and the base fluid, respectively. The experimental thermophysical characteristics of the regular pure liquid (water) and copper oxide (CuO) nanoparticles are numerically illustrated in Table 1.

We introduce the following dimensionless variables:

$$\begin{aligned} u_a &= \frac{A_a x_a}{1 - \alpha_A t^*} F'(\zeta), v_a = \frac{B_a y_a}{1 - \alpha_A t^*} G'(\zeta), \zeta = \left(\frac{A_a}{v_f (1 - \alpha_A t^*)} \right)^{1/2} z_a, K_a = (1 - \alpha_A t^*) K^*, \\ w_a &= - \left(\frac{v_f A_a}{1 - \alpha_A t^*} \right)^{1/2} (F + C_a G) \alpha_A t^* < 1, S(\zeta) = \frac{T_a - T_\infty}{T_w - T_\infty}, \lambda_a = \lambda^* (1 - \alpha_A t^*)^{1/2}. \end{aligned} \tag{8}$$

Table 1
The thermophysical features of the (CuO-water) nanofluid [56].

Physical properties	Water	CuO
c_p (J/kgK)	4179	540
ρ (kg/m ³)	997.1	6500
k (W/mK)	0.613	18
Pr	6.2	-

Here, $C_a = \frac{B_a}{A_a}$ called the nodal/saddle stagnation point.

The similarity equations here are derived as follows:

$$\begin{aligned} \frac{\mu_{nf}/\mu_f}{\rho_{nf}/\rho_f} F''' + (F + C_a G)F'' + \alpha_A \left(1 - F' - \frac{\zeta}{2} F'' \right) + (1 - F^2) \\ + \frac{\mu_{nf}/\mu_f}{\rho_{nf}/\rho_f} m_a (1 - F') = 0 \end{aligned} \tag{9}$$

$$\begin{aligned} \frac{\mu_{nf}/\mu_f}{\rho_{nf}/\rho_f} G''' + (F + C_a G)G'' + \alpha_A \left(1 - G' - \frac{\zeta}{2} G'' \right) + C_a (1 - G^2) \\ + \frac{\mu_{nf}/\mu_f}{\rho_{nf}/\rho_f} m_a (1 - G') = 0 \end{aligned} \tag{10}$$

$$\frac{k_{nf}/k_f}{Pr(\rho c_p)_{nf}/(\rho c_p)_f} S'' + (F + C_a G)S' - \alpha_A \frac{\zeta}{2} S' = 0 \tag{11}$$

along with subject BCs.

$$\left. \begin{aligned} F(\zeta) &= 0, G(\zeta) = 0, F'(\zeta) = \delta_a F''(\zeta), G'(\zeta) = \delta_a G''(\zeta), S(\zeta) = 1 \text{ at } \zeta = 0, \\ F'(\zeta) &\rightarrow 1, G'(\zeta) \rightarrow 1, S(\zeta) \rightarrow 0 \text{ as } \zeta \rightarrow \infty. \end{aligned} \right\} \tag{12}$$

The dimensionless parameters involved in the above similarity equations are the following as $m_a = \frac{v_a v_f}{K^* A_a}$ is the porous media permeability parameter and $\delta_a = \frac{2 - \sigma_u}{\sigma_u} \lambda^* \left(\frac{A_a}{v_f} \right)^{1/2}$ called the dimensionless velocity slip factor.

The engineering physical quantities of practical interest are the friction factor in x_a and y_a axes are denoted by C_{fx_a} and C_{fy_a} while the local Nusselt number Nu_{x_a} is demarcated as:

$$\begin{aligned} C_{fx_a} &= \frac{\mu_{nf}}{\rho_f u_{exa}^2} \left(\frac{\partial u_a}{\partial z_a} \right) \Big|_{z_a=0}, C_{fy_a} = \frac{\mu_{nf}}{\rho_f v_{eya}^2} \left(\frac{\partial v_a}{\partial z_a} \right) \Big|_{z_a=0}, \\ Nu_{x_a} &= - \frac{x_a k_{nf}}{k_f (T_w - T_\infty)} \left(\frac{\partial T_a}{\partial z_a} \right) \Big|_{z_a=0}, \end{aligned} \tag{13}$$

Further, by plugging Eq. (8) into Eq. (13), we get.

$$\begin{aligned} Re_{x_a}^{1/2} C_{fx_a} &= \frac{\mu_{nf}}{\mu_f} F''(0), Re_{y_a}^{1/2} C_{fy_a} = \frac{1}{\sqrt{C_a}} \frac{\mu_{nf}}{\mu_f} G''(0), \\ Re_{x_a}^{1/2} Nu_{x_a} &= - \frac{k_{nf}}{k_f} S'(0). \end{aligned} \tag{14}$$

where $Re_{x_a} = \frac{u_{exa} x_a}{v_f}$ and $Re_{y_a} = \frac{v_{eya} y_a}{v_f}$ are called the local Reynolds numbers.

3. Results and discussions

Due to authentication, appropriateness, and strong support of the precise numerical outcomes, a comparison was made among the existing outcomes of the shear stress along with the axial and lateral directions and heat transfer for the upper branch owing to the various distinct value of φ with those of Bhattacharyya and Gupta [57] and Dinarvand et al. [58] without the influence of m_a, α_a and δ_a as decorated in Table 2. Here, we have shown the assessment for the pure working fluid $\varphi = 0$ as well as for the posited

case of the copper-oxide nanoparticle parameter $\varphi = (0.10, 0.20)$. In the comparison, we noticed a remarkable toning and respectable settlement between the existing and available published works. In addition, this excellent confirmation of the code can give us extreme confidence that our acquired unavailable double branch outcomes of the problem are found perfectly right.

Apart from this, the current problem included the following four dissimilar influential parameters such as the porous media permeability parameter m_a , the time-dependent parameter α_a , the velocity slip factor δ_a , and the nanoparticles volume fraction φ . The physical rule of these distinguished parameters on the gradients (shear stress along with the axial and lateral directions and heat transfer) as well as the velocities profiles in both directions and temperature distribution fields are elucidated in Figs. 2 to 13. For the simulations of the model, we have set the values of the influential constraints throughout the document in the following measures such as $\alpha_A = -2.5, m_a = 0.15, \delta_a = 0.5$ and $\varphi = 0.03$. In all the graphs, the solid black lines signify the upper branch solution (UBS) and the dash black lines correspond to the lower branch solution (LBS), whereas for simplicity we can rewrite similar things by the corresponding UBS and LBS, respectively. Moreover, the location or position in all the available designed graphs is called the bifurcation or critical point (BP or CP), whereas the UBS and LBS can merge. This CP was further highlighted via the solid grey, red and blue balls (see Figs. 2 to 7), whereas for each distinct parameter value it is changed in the graphs.

To see the behavior of the fluid flow dynamics and heat transfer characteristics in a more explicit way, therefore, Tables 3 and 4 are constructed. In particular, Table 3 elucidates the number of calculated computational values of the friction factor in both axial and lateral directions for the assorted choices of the selected controlling constraints when $\alpha_A = -2.5$ and $C_a = 0.0005$. From the outcomes, it is seen that the increasing impact of φ can improve the friction factor in the lateral direction for the UBS while for the LBS it is decreased. Oppositely, the friction factor along the axial direction can behave completely change for the UBS and as well as for LBS with a higher value of φ . In physical interpretations, the concentration of fluid is decelerated due to the larger influences of nanoparticles which moderates the fluid viscosity and reinforces the inertial which is ultimately a decisive factor for a decrement in the velocity field. As a conclusion statement, the velocity and shear stress obey the law of inverse proportionality, hence, the friction factor upsurges with higher φ . In addition, the shear stress along the axial direction enriches monotonically due to successive rules of m_a but the shear stress along the lateral direction shows that the tendency of the curves goes down for

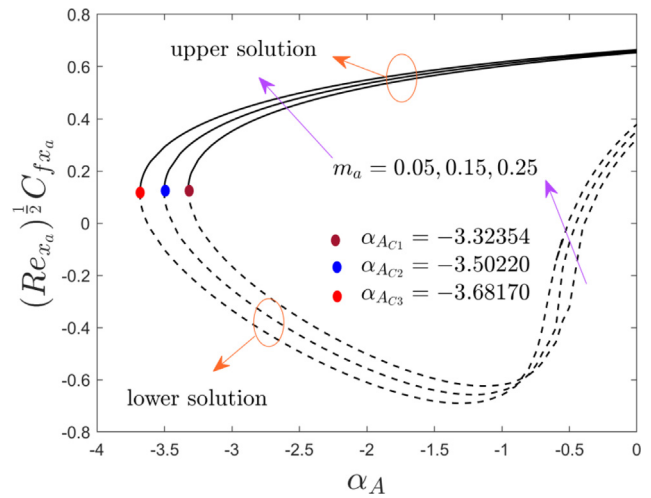


Fig. 2. Variation of the shear stress along the lateral direction with α_a for several values of m_a .

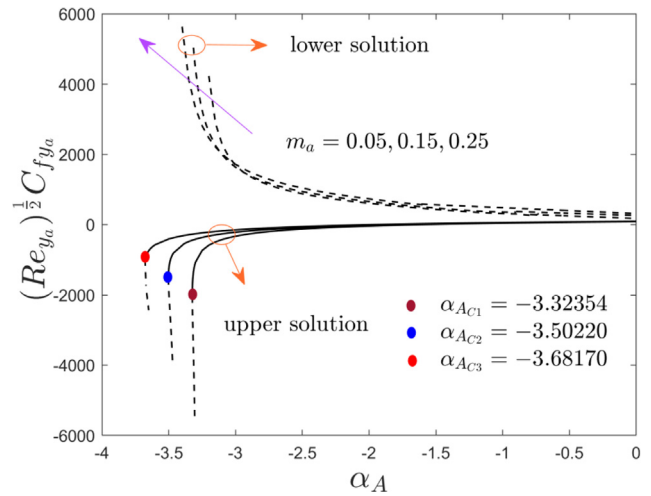


Fig. 3. Variation of the friction factor along the axial direction with α_a for varying values of m_a .

Table 2

Comparison of present outcomes for the upper branch solution with published available works when $m_a = 0, \alpha_A = 0$ and $\delta_a = 0$.

φ	Bhattacharyya and Gupta [57]		Dinarvand et al. [58]		Present results	
	$C_a = -0.5$	$C_a = 0.5$	$C_a = -0.5$	$C_a = 0.5$	$C_a = -0.5$	$C_a = 0.5$
$Re_{x_a}^{1/2} C_{f_{x_a}}$						
0.0	1.231289	1.267911	1.2325	1.2681	1.232534	1.268145
0.1	-	-	1.6285	1.6657	1.628513	1.665767
0.2	-	-	2.0910	2.1530	2.091024	2.153078
$Re_{y_a}^{1/2} C_{f_{y_a}}$						
0.0	0.055751	0.499358	0.05576	0.4993	0.055764	0.499389
0.1	-	-	0.07329	0.6557	0.073294	0.655767
0.2	-	-	0.09477	0.8477	0.094772	0.847745
$Re_{x_a}^{1/2} Nu_{x_a}$						
0.0	1.123501	1.330245	1.12377	1.3301	1.123776	1.330135
0.1	-	-	1.29052	1.4956	1.290524	1.495643
0.2	-	-	1.45452	1.7386	1.454522	1.738632

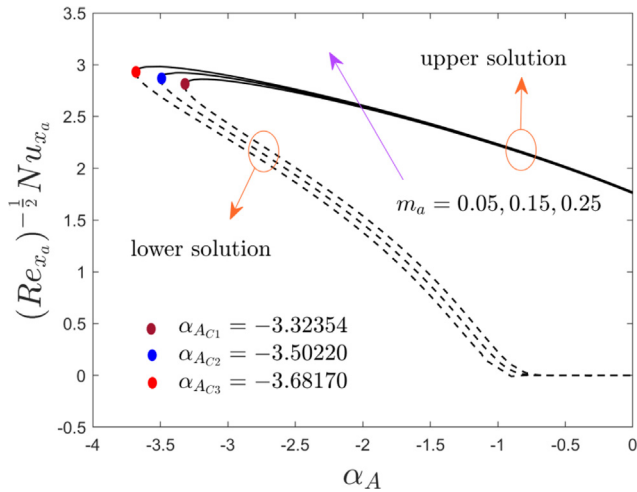


Fig. 4. Variation of the heat transfer with α_a for varying values of m_a .

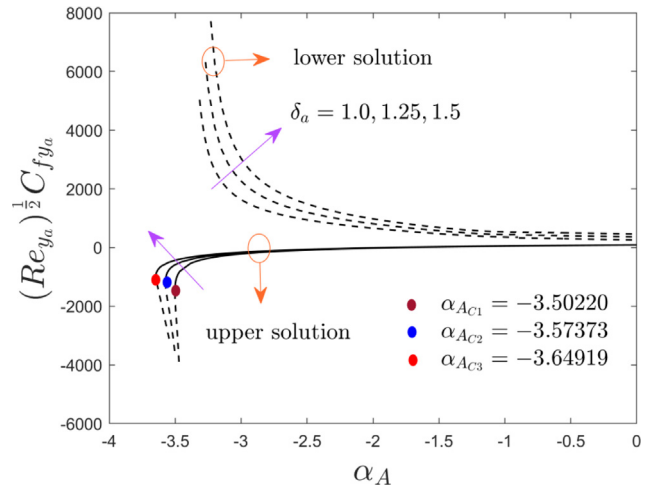


Fig. 6. Variation of the shear stress along the axial direction with α_a for several values of δ_a .

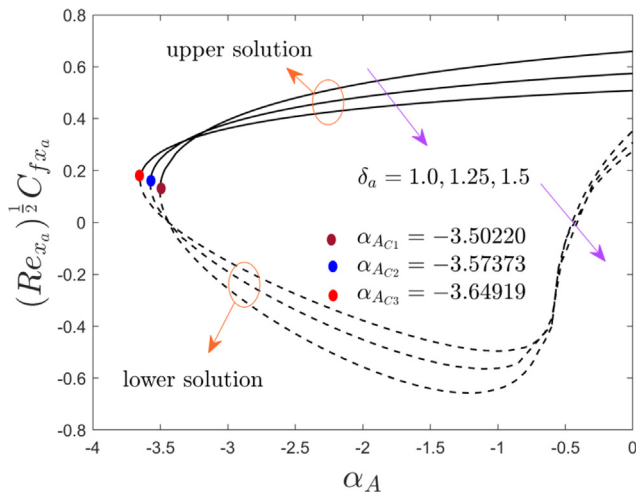


Fig. 5. Variation of the shear stress along the lateral direction with α_a for several values of δ_a .

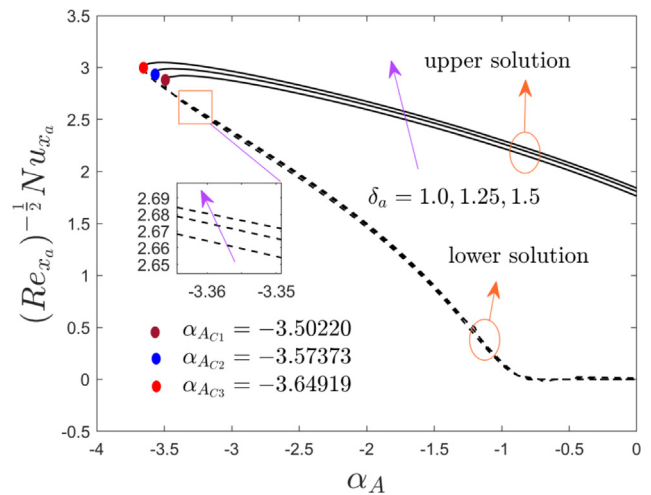


Fig. 7. Variation of the heat transfer with α_a for varying values of δ_a .

the LBS and upsurges for the UBS due to incremental changes in m_a . However, the larger value of δ_a decelerates the friction factor in the direction of lateral for the UBS and escalates for the LBS while the effects of δ_a are entirely changed for the shear stress along the axial direction. Also, the heat transfer arithmetic number of values for the gigantic number of selected parameters is portrayed in Table 4 when $\alpha_A = -2.5$, $C_a = 0.0005$ and $Pr = 6.2$. The heat transfer is lesser for the parameter m_a as compared to the other influential parameters. Moreover, the heat transfer continuously improves for the UBS as well as LBS due to the augmentation in the values of φ and δ_a . Physically, the huge impact of φ can mainly develops the key modes such as thermal conductivity, and as a response; the rate of heat transfer is augmented.

Figs. 2 to 7 illustrate the characteristics of the multiple (UB and LB) solutions of the existing problem and are discussed in terms of the shear stress along with axial and lateral directions and heat transfer of the (CuO-water) based nanofluid versus α_A for the dissimilar values of m_a and δ_a . In these figures, it can be seen that the UBS and LBS are found for the equations (9) to (11) in the range $\alpha_A > \alpha_{Ac}$, a single result originates when $\alpha_A = \alpha_{Ac}$ and no result exists when $\alpha_A < \alpha_{Ac}$, whereas, α_{Ac} is the critical value of

α_{Ac} by which the UBS and LBS merged. For more details, Figs. 2, 3, and 4 exemplify the shear stress along with axial and lateral directions and heat transfer owing to the influence of m_a for the UBS as well as for the LBS when the rest of the parameters are taken to be fixed. The outcomes of the shear stress along both directions for the UBS enriches due to m_a while the shear stress along with the respective both directions for the LBS declines and rises in the range of $-\infty < m_a < -0.85$ and $-3.15 < m_a < -2.85$ then the gradients start distinct behavior for the same branch solution. In addition, the breaking of the LBS curves at some finite value α_0 of α_A due to the significant impact of the unsteadiness and porous media permeability comprising the copper oxide nanoparticles as well (see Fig. 3). Besides, the heat transfer for the UBS curves elevates with larger m_a and decelerates for the LBS in the range of $-\infty < m_a < -0.75$ and then goes to zero as we move forward from the flow of decelerating towards the accelerating. The critical values are the following such as -3.32354 , -3.50220 , and -3.68170 for the three distinct selected choices of m_a (0.05, 0.15, 0.25), respectively. From this behavior, it is further detected that the magnitude of the BP is accelerated with m_a , therefore, the separations of the boundary layer diminished.

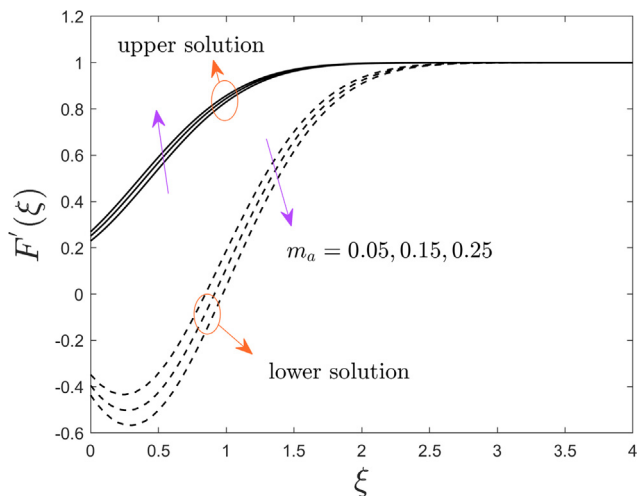


Fig. 8. Deviation of the velocity profiles along the lateral direction for several values of m_a .

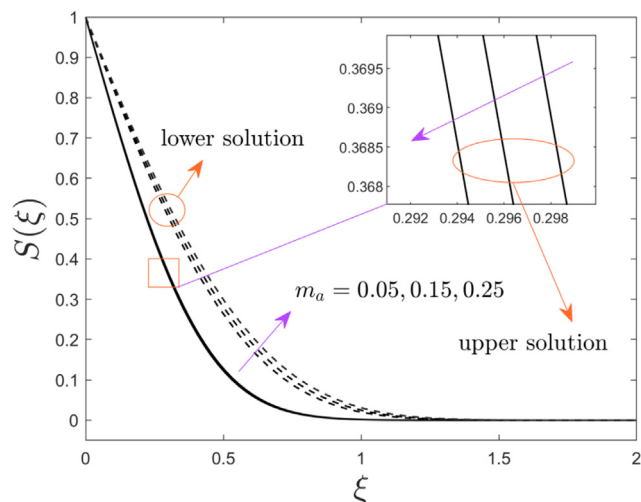


Fig. 10. Deviation of the temperature profiles for several values of m_a .

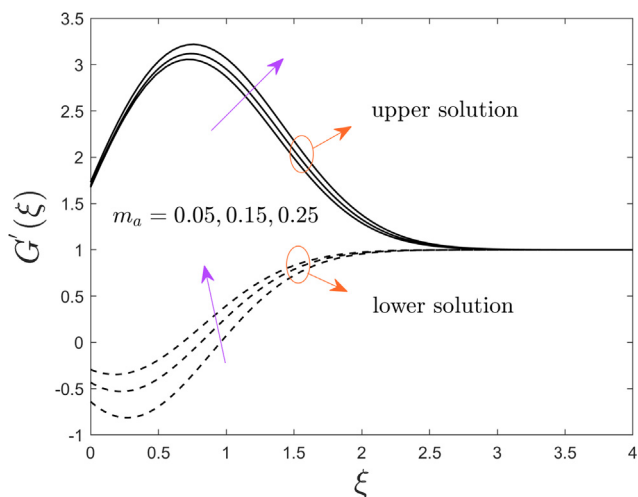


Fig. 9. Deviation of the velocity profiles along the axial direction for several values of m_a .

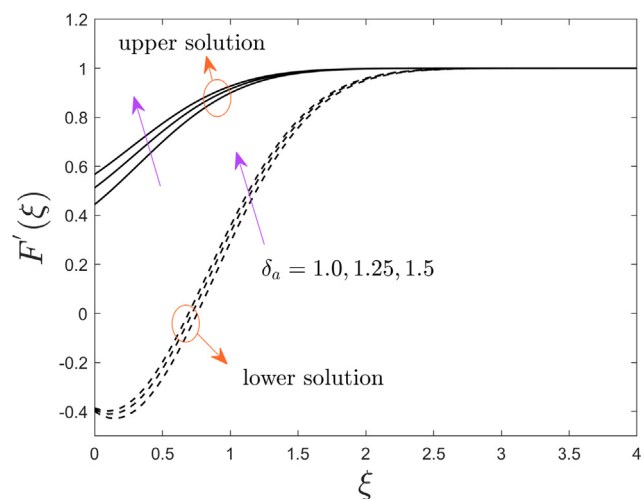


Fig. 11. Deviation of the velocity profiles along the lateral direction for several values of δ_a .

Furthermore, the influences of δ_a on the shear stress along with axial and lateral directions and heat transfer for both solution branches are highlighted in Figs. 5, 6, and 7, respectively. Outcomes divulge that the shear stress along the lateral direction accelerated to near the critical value for the UBS and then abruptly begin the deceleration for the same solution branch if we move to escalate the impacts of δ_a while for the LBS it performs the change in each specific range of portion against α_A . The heat transfer and the shear stress along the axial direction are improved significantly for both solutions (UBS and LBS) due to the augmentation in δ_a while the LBS for the shear stress is similarly broken due to the presence of the porous medial permeability, unsteadiness, and nanoparticles impressions. Generally, in the phenomenon of Maxwell slip BCs, the reduction of the fluid speed creates shrinkage in the velocity which is happened due to the velocity of the sheet and fluids are not the same at the sheet surface, as a result, the shear stress is augmented near the bifurcation values. For the increasing value of δ_a , the bifurcation values magnitude-wise escalate. In this

respect, the behavior of the boundary layer separation shrinkages because of the larger improvement in δ_a .

Figs. 8, 9, and 10 depict the inspiration of the porous media permeability parameter m_a on the velocity profiles along with axial and lateral directions and the temperature distribution profiles of the (CuO-water) nanofluid, respectively. As m_a upsurges, the velocity field $F'(\xi)$ escalates for UBS and decelerates for LBS, whereas the velocity profile $G'(\xi)$ remarkably enriches for both branch solutions. On the other hand, the temperature distribution $S(\xi)$ elevates for the UBS and declines for the LBS owing to its larger m_a . In physical explanations, the larger implementation of the porous media permeability parameter can build improvement in the surface of the sheet (like in shape,) due to which the flow of fluid particles improves; as a result, the velocity profile enlarges. In addition, the inclusion of m_a enhances the momentum boundary layer but reduces the thermal boundary layer.

The deviations of δ_a on the velocity profiles in both the axial and lateral directions and the temperature distribution profiles of the (CuO-water) nanofluid against ξ for the two dissimilar branches

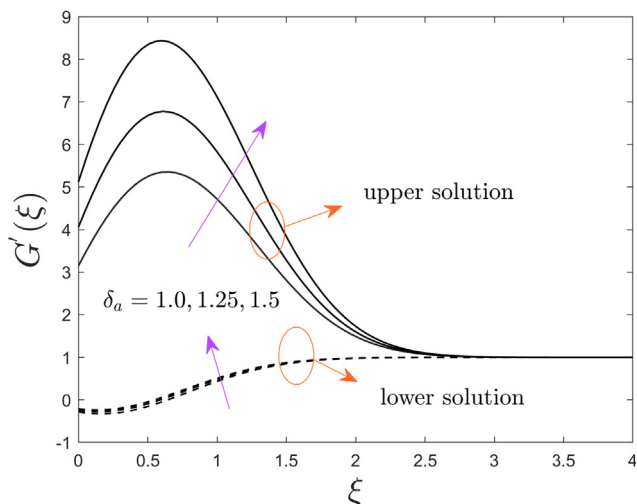


Fig. 12. Deviation of the velocity profiles along the axial direction for several values of δ_a .

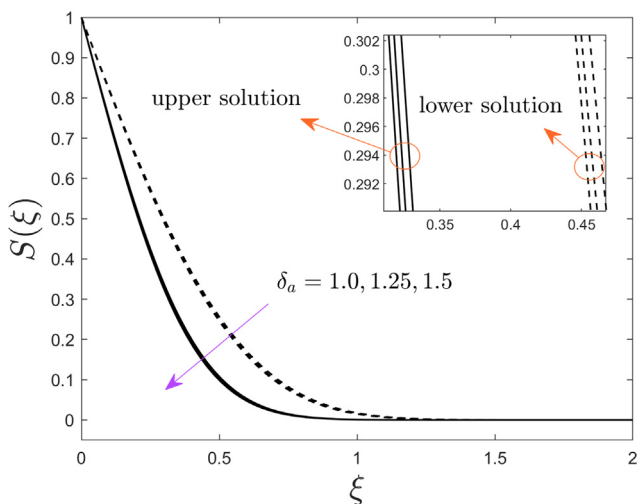


Fig. 13. Deviation of the temperature profiles for several values of δ_a .

Table 3

The friction factor numerical values in both directions for the sundry values of the parameters when $\alpha_A = -2.5$ and $C_a = 0.0005$.

φ	m_a	δ_a	$\frac{\mu_{inf}}{\mu_f} F''(0)$		$(C_a)^{-1/2} \frac{\mu_{inf}}{\mu_f} G''(0)$	
			Upper solution	Lower solution	Upper solution	Lower solution
0.025	0.15	0.5	0.5318	-0.8404	-40.7730	161.1647
0.030			0.5408	-0.8504	-41.7726	163.2253
0.035			0.5498	-0.8606	-42.7703	165.3223
0.025	0.05	0.025	0.4860	-0.7417	-60.4177	159.6100
	0.15		0.5318	-0.8404	-40.7730	161.1647
	0.25		0.5712	-0.9313	-27.5527	164.9762
0.025	0.15	0.5	0.5318	-0.8404	-40.7730	161.1647
		1.0	0.4717	-0.4254	-36.4681	72.2530
		1.5	0.4018	-0.2734	-34.1613	43.3244

Table 4

The heat transfer $-\frac{k_{eff}}{k_f} S'(0)$ numerical values for the sundry values of the parameters when $\alpha_A = -2.5$, $C_a = 0.0005$ and $Pr = 6.2$.

φ	m_a	δ_a	$-\frac{k_{eff}}{k_f} S'(0)$	
			Upper solution	Lower solution
0.025	0.15	0.5	2.5946	1.8432
0.030			2.6125	1.8575
0.035			2.6305	1.8717
0.025	0.05	0.025	2.5742	1.9120
	0.15		2.5946	1.8432
	0.25		2.6119	1.7765
0.025	0.15	0.5	2.5946	1.8432
		1.0	2.7304	1.9204
		1.5	2.8116	1.9612

(UB and LB) outcomes are bounded schematically in Figs. 11, 12, and 13, respectively. With the escalation of δ_a , the velocity profiles in both axes of directions continuously heighten for the UBS as well as for the LBS. There is realized a reduction in the temperature distribution profiles for both solution branches with the superior value of δ_a . The general reason is that the magnification in the value of δ_a diminishes the distance between the surface of the sheet and the far-field boundary temperature which additionally transported inferior or negligible heat to the fluid particles from the wall surface, as a result, lessens the fluid temperature as well as the temperature distribution profiles. Moreover, the thermal boundary layer is also declined with δ_a .

4. Conclusion

The influence of generalized slip effects along with exploration of boundary stratum of 3D stagnation-point flow induced by a copper oxide nanoparticle into the based working fluid (water) past a horizontal plane surface embedded in a porous medium was investigated in the given problem. The similarity equations (9) to (11) subjected to BCs (12) are reduced from the well-known posited governing PDEs via utilizing the self-similarity variables. These equations additionally comprised distinct influential controlling parameters, however, the impact of each distinguished parameter on the shear stress along with axial and lateral directions and heat transfer were portrayed through distinct portraits and as well as in the form of tables. Moreover, it is established that for a specific set of non-dimensional factors, the gradients reveal the multiple (UB and LB) outcomes over a prolonged region of the unsteadiness parameter. The key outcomes of the numerical analysis are emphasized as follows:

- The friction factor along axial and lateral directions elevates for UBS and reduces for LBS due to the larger value of m_a , whereas, the heat transfer extraordinarily heightens for the stable branch solution and diminished for the unstable branch.
- The inclusion of φ decelerates the friction factor in the axial direction for the UBS and escalates for the LBS, whereas, the shear stress along the lateral direction behaves oppositely like the shear stress along the axial direction but heat transfer is monotonically enhanced.
- The MBL thickness strengthens for the higher value of m_a meanwhile the thickness of the thermal boundary layer shrinkages.
- The increasing value of δ_a improves the heat transfer and the magnitude of the friction factor in the axial direction for the UBS and LBS while the magnitude of the friction factor along the lateral direction behaves distinctly for both solution branches.
- In both directions, the velocity profile augments for the higher impact of δ_a while the temperature distribution profile diminishes.

Declaration of Competing Interest

The authors declare that they have no known competing financial interests or personal relationships that could have appeared to influence the work reported in this paper.

Acknowledgments

The author (Z. Raizah) extends their appreciation to the Deanship of Scientific Research at King Khalid University, Abha, Saudi Arabia, for funding this work through the Research Group Project under Grant Number (RGP.1/254/42).

References

- [1] Choi SU, Eastman JA. Enhancing thermal conductivity of fluids with nanoparticles. In: Proceedings of the international mechanical engineering congress and exhibition, San Francisco, CA, USA, 12–17; November 1995..
- [2] Khanafer K, Vafai K, Lightstone M. Buoyancy-driven heat transfer enhancement in a two-dimensional enclosure utilizing nanofluids. *Int J Heat Mass Transf* 2003;46(19):3639–53.
- [3] Oztop HF, Abu-Nada E. Numerical study of natural convection in partially heated rectangular enclosures filled with nanofluids. *Int J Heat Fluid Flow* 2008;29(5):1326–36.
- [4] Motsumi TG, Makinde OD. Effects of thermal radiation and viscous dissipation on boundary layer flow of nanofluids over a permeable moving flat plate. *Phys Scr* 2012;86(4):045003. doi: <https://doi.org/10.1088/0031-8949/86/04/045003>.
- [5] Farooq M, Khan MI, Waqas M, Hayat T, Alsaedi A, Khan MI. MHD stagnation point flow of viscoelastic nanofluid with non-linear radiation effects. *J Mol Liq* 2016;221:1097–103.
- [6] Naramgari S, Sulochana C. MHD flow over a permeable stretching/shrinking sheet of a nanofluid with suction/injection. *Alex Eng J* 2016;55(2):819–27.
- [7] Shagaiya Daniel Y, Abdul Aziz Z, Ismail Z, Salah F. Effects of thermal radiation, viscous and Joule heating on electrical MHD nanofluid with double stratification. *Chin J Phys* 2017;55(3):630–51.
- [8] Kumar N, Sonawane SS, Sonawane SH. Experimental study of thermal conductivity, heat transfer and friction factor of Al_2O_3 based nanofluid. *Int J Commun Heat Mass Transf* 2018;90:1–10.
- [9] Moghadasi R, Rostami A, Hemmati-Sarapardeh A. Application of nanofluids for treating fines migration during hydraulic fracturing: Experimental study and mechanistic understanding. *Adv Geo-Energy Res* 2019;3(2):198–206.
- [10] Abbas SZ, Khan WA, Sun H, Irfan M, Khan MI, Waqas M. Von Kármán swirling analysis for modeling Oldroyd-B nanofluid considering cubic autocatalysis. *Phys Scr* 2020;95(1):015206. doi: <https://doi.org/10.1088/1402-4896/ab450f>.
- [11] Turkyilmazoglu M. Suspension of dust particles over a stretchable rotating disk and two-phase heat transfer. *Int J Multiphase Flow* 2020;127:103260. doi: <https://doi.org/10.1016/j.ijmultiphaseflow.2020.103260>.
- [12] Khan U, Zaib A, Shah Z, Baleanu D, Sherif E-S, M. Impact of magnetic field on boundary-layer flow of Sisko liquid comprising nanomaterials migration through radially shrinking/stretching surface with zero mass flux. *J Mater Res Tech* 2020;9(3):3699–709.
- [13] Ramesh K, Khan SU, Jameel M, Khan MI, Chu Y-M, Kadry S. Bioconvection assessment in Maxwell nanofluid configured by a Riga surface with nonlinear

- thermal radiation and activation energy. *Surfaces Interfaces* 2020;21:100749. doi: <https://doi.org/10.1016/j.surfin.2020.100749>.
- [14] Turkyilmazoglu M. On the transparent effects of Buongiorno nanofluid model on heat and mass transfer. *Eur Phys J Plus* 2021;136:376.
 - [15] Khan MI, Qayyum S, Shah F, Kumar RN, Punith Gowda RJ, Prasannakumara BC, et al. Marangoni convective flow of hybrid nanofluid ($MnZnFe_2O_4-NiZnFe_2O_4-H_2O$) with Darcy Forchheimer medium. *Ain Shams Eng J* 2021;12:3931–8.
 - [16] Hemmat Esfe M, Bahiraei M, Torabi A, Valadkhani M. A critical review on pulsating flow in conventional fluids and nanofluids: Thermo-hydraulic characteristics. *Int Comm Heat Mass Transf* 2021;120:104859. doi: <https://doi.org/10.1016/j.icheatmasstransfer.2020.104859>.
 - [17] Turkyilmazoglu M. Heat transfer enhancement feature of the non-Fourier Cattaneo-Christov heat flux model. *J Heat Transf* 2021;143(9):094501.
 - [18] Bahiraei M, Mazaheri N. Using spiral channels for intensification of cooling process in an innovative liquid block operated with a biologically produced nanofluid: First and second law analyses. *Chem Eng Processing- Process Intensification* 2021;162:108326. doi: <https://doi.org/10.1016/j.cep.2021.108326>.
 - [19] Song Y-Q, Ali Khan S, Imran M, Waqas H, Ullah Khan S, Ijaz Khan M, et al. Applications of modified Darcy law and nonlinear thermal radiation in bioconvection flow of micropolar nanofluid over an off centered rotating disk. *Alexandria Eng J* 2021;60(5):4607–18.
 - [20] Khan U, Zaib A, Ishak A, Abu Bakar S, Muhammad T. Numerical simulations of bio-convection in the stream-wise and cross-flow directions comprising nanofluid conveying motile microorganism: Analysis of multiple solutions. *Int J Comput Meth* 2021;2150058..
 - [21] Chu Y-M, Nazeer M, Khan MI, Hussain F, Rafi H, Qayyum S, et al. Combined impacts of heat source/sink, radiative heat flux, temperature dependent thermal conductivity on forced convective Rabinowitsch fluid. *Int Comm Heat Mass Transf* 2021;120:105011. doi: <https://doi.org/10.1016/j.icheatmasstransfer.2020.105011>.
 - [22] Bahiraei M, Mazaheri N, Hanooni M. Employing a novel crimped-spiral rib inside a triple-tube heat exchanger working with a nanofluid for solar thermal applications: Irreversibility characteristics. *Sustainable Energy Tech Asses* 2022;52:102080. doi: <https://doi.org/10.1016/j.seta.2022.102080>.
 - [23] Mazaheri N, Bahiraei M, Razi S. Second law performance of a novel four-layer microchannel heat exchanger operating with nanofluid through a two-phase simulation. *Powder Tech* 2022;396:673–88.
 - [24] Navier CLMH. Mémoire sur les lois du mouvement des fluids. *Mémoires de l'Académie des sciences* 1827;6:389–91.
 - [25] Maxwell JC. On stresses in rarefied gases arising from inequalities of temperature. *Proceed Royal Soc London* 1878;27:304–8.
 - [26] Matthews MT, Hill JM. Flow around nanospheres and nanocylinders. *Q J Mech Appl Math* 2006;59(2):191–210.
 - [27] Wang CY. Flow Due to stretching boundary with partial slip—An Exact solution of the Navier Stokes equation. *Chemical Eng Sci* 2002;57:3745–7.
 - [28] Thompson PA, Troian SM. A general boundary condition for liquid flow at solid surfaces. *Nature* 1997;389(6649):360–2.
 - [29] Matthews MT, Hill JM. Newtonian flow with nonlinear Navier boundary condition. *Acta Mech* 2007;191(3–4):195–217.
 - [30] Sajid M, Ali N, Abbas Z, Javed T. Stretching flows with general slip condition. *Int J Modern Phys B* 2010;24(30):5939–47.
 - [31] Khan WA, Uddin MJ, Ismail AIM, Abbott D. Hydrodynamic and thermal slip effect on double-diffusive free convective boundary layer flow of a nanofluid past a flat vertical plate in the moving free stream. *PLoS ONE* 2013;8(3):e54024. doi: <https://doi.org/10.1371/journal.pone.0054024>.
 - [32] Power H, Soavi J, Kantachuesiri P, Nieto C. The effect of Thompson and Troian's nonlinear slip condition on Couette flows between concentric rotating cylinders. *Z Angew Math Phys* 2015;66:2703–18.
 - [33] Khashi'ie NS, Arifin NM, Pop I, Nazar R, Hafidzuddin EH, Wahi N. Three-dimensional hybrid nanofluid flow and heat transfer past a permeable stretching/shrinking sheet with velocity slip and convective condition. *Chin J Phys* 2020;66:157–71.
 - [34] Hiemenz K. Die Grenzschicht an einem in den gleichförmigen Flüssigkeitsstrom eingetauchten geraden Kreiszylinder. *Dingler's Polytech J* 1911;326:321–4.
 - [35] Homann F. Der Einfluss grosser Zähigkeit bei der Stromung um den Zylinder und um die Kugel. *Z Angew Math Mech* 1936;16:153–64.
 - [36] Mahapatra TR, Gupta AS. Heat transfer in stagnation-point flow towards a stretching sheet. *Heat Mass Transf* 2002;38(6):517–21.
 - [37] Mahapatra TR, Gupta AS. Stagnation-point flow towards a stretching surface. *Can J Chem Eng* 2003;81(2):258–63.
 - [38] Wang CY. Stagnation flow towards a shrinking sheet. *Int J Non Linear Mech* 2008;43(5):377–82.
 - [39] Lok YY, Ishak A, Pop I. MHD stagnation-point flow towards a shrinking sheet. *Int J Numer Meth Heat Fluid Flow* 2011;21:61–72.
 - [40] Bachok N, Ishak A, Pop I. Stagnation-point flow over a stretching/shrinkingsheet in a nanofluid. *Nanoscale Res Lett* 2011;6:623.
 - [41] Mabood F, Pochai N, Shateyi S. Stagnation point flow of nanofluid over a moving plate with convective boundary condition and magnetohydrodynamics. *J Eng* 2016;2016:1–11.
 - [42] Nithyadevi N, Gayathri P, Sandeep N. Boundary stratum exploration of unsteady 3D MHD stagnation point flow of Al–Cu water nanofluid. *Int J Mech Sci* 2017;131–132:827–35.
 - [43] Turkyilmazoglu M. Stagnation-point flow and heat transfer over stretchable plates and cylinders with an oncoming flow: Exact solutions. *Chem Eng Sci* 2021;238:116596. doi: <https://doi.org/10.1016/j.ces.2021.116596>.

- [44] Ahmad S, Pop I. Mixed convection boundary layer flow from a vertical flat plate embedded in a porous medium filled with nanofluids. *Int Commun Heat Mass Transf* 2010;37(8):987–91.
- [45] Sheikholeslami M, Ziaabakhsh Z, Ganji DD. Transport of magnetohydrodynamic nanofluid in a porous media. *Coll Surf A Phys Eng Asp* 2017;520:201–12.
- [46] Abu Bakar S, Arifin N, Md Ali F, Bachok N, Nazar R, Pop I. A stability analysis on mixed convection boundary layer flow along a permeable vertical cylinder in a porous medium filled with a nanofluid and thermal radiation. *Appl Sci* 2018;8(4):483. doi: <https://doi.org/10.3390/app8040483>.
- [47] Turkyilmazoglu M. Velocity slip and entropy generation phenomena in thermal transport through metallic porous channel. *J Non-Equil Thermodynamics* 2020;45(3):247–56.
- [48] Rashad AM, Khan WA, EL-Kabeir SMM, EL-Hakiem AMA. Mixed convective flow of micropolar nanofluid across a horizontal cylinder in saturated porous medium. *Appl Sci* 2019;9(23):5241. doi: <https://doi.org/10.3390/app9235241>.
- [49] Haq RU, Raza A, Algehyne EA, Tlili I. Dual nature study of convective heat transfer of nanofluid flow over a shrinking surface in a porous medium. *Int J Commun Heat Mass Transf* 2020;114:104583. doi: <https://doi.org/10.1016/j.icheatmasstransfer.2020.104583>.
- [50] Bakar SA, Arifin NM, Khashi'ie NS, Bachok N. Hybrid nanofluid flow over a permeable shrinking sheet embedded in a porous medium with radiation and slip impacts. *Mathematics* 2021;9: 878.
- [51] Nisar KS, Khan U, Zaib A, Khan I, Baleanu D. Numerical simulation of mixed convection squeezing flow of a hybrid nanofluid containing magnetized ferroparticles in 50%: 50% of ethylene glycol–water mixture base fluids between two disks with the presence of a non-linear thermal radiation heat flux. *Front Chem* 2020:792.
- [52] Wang F, Rani SP, Sarada K, Punith Gowda RJ, Umair khan, Zahran HY, et al. The effects of nanoparticle aggregation and radiation on the flow of nanofluid between the gap of a disk and cone. *Case Stud Therm Eng* 2022;33:101930. doi: <https://doi.org/10.1016/j.csite.2022.101930>.
- [53] Khan U, Zaib A, Ishak A, Waini I, Sherif ESM, Pop I. Forced convective MHD flow of Reiner-Philippoff fluid induced by hybrid nanofluid past a nonlinear moving sheet with nonlinear heat sink/source. *Waves Random Complex Medium* 2022:1–22.
- [54] Pop I, Khan U, Zaib A, Ishak A. Hybrid nanofluid flow past an unsteady porous stretching/shrinking sheet with Newtonian heating in a porous medium. *J Porous Media* 2022.
- [55] Zainal NA, Nazar R, Naganthran K, Pop I. Unsteady three-dimensional MHD non-Axisymmetric Homann stagnation point flow of a hybrid nanofluid with stability analysis. *Mathematics* 2020;8(5):784. doi: <https://doi.org/10.3390/math8050784>.
- [56] Nayak B, Mishra SR. Squeezing flow analysis of CuO–water and CuO–kerosene-based nanofluids: a comparative study. *Pramana – J Phys* 2021;95:29.
- [57] Bhattacharyya S, Gupta AS. MHD flow and heat transfer at a general three-dimensional stagnation point. *Int J Non-Linear Mech* 1998;33(1):125–34.
- [58] Dinarvand S, Hosseini R, Damangir E, Pop I. Series solutions for steady three-dimensional stagnation point flow of a nanofluid past a circular cylinder with sinusoidal radius variation. *Meccanica* 2013;48(3):643–52.